ELSEVIER

Applied Mathematical Modelling 23 (1999) 915–932

APPLIED MATHEMATICAL MODELLING

www.elsevier.nl/locate/apm

Numerical investigation of vortical evolution in a backward-facing step expansion flow

T.P. Chiang, Tony W.H. Sheu *, C.C. Fang

Department of Naval Architecture and Ocean Engineering, National Taiwan University, 73 Chou-Shan Road, Taipei, Taiwan, ROC

Received 16 September 1997; received in revised form 25 March 1999; accepted 16 April 1999

Abstract

A numerical investigation of laminar flow over a backward-facing step is presented for the Reynolds number in the range of $50 \leqslant \mathrm{Re} \leqslant 2500$. The objective of this numerical investigation is to add to the existing knowledge of the backward-facing step flow to deepen our understanding of the expansion flow structure. We proceed with the analysis by verifying the computer code through the Pearson vortex problem. We then perform a parametric study by varying the Reynolds number, with the aim of determining whether or not there exists a critical Reynolds number, above which reattachment length on the channel floor decreases. We also concentrate on subjects that have been little explored in the flow, examples of which are the onset of a single vortex in the primary eddy and how the recirculating bubble containing flow reversals is torn into smaller eddies. Eddy distortion, leading to mobile saddle points, and the merging of eddies are also discussed in this study.

Nomenclature

u_i	velocity component along i-direction
p	pressure
x_m	coordinate along m-direction
t	time
v	kinematic viscosity
$U_{\max}$	maximum inlet channel velocity ($\equiv 1$)
U_{mean}	mean inlet channel velocity ($\equiv \frac{2}{3}$)
h	height of the upstream channel ($\equiv 1$)
Re^*	Reynolds number defined by $\mathrm{Re}^* = U_{\max}h/v$
Re	Reynolds number defined by Armaly et al. ($\equiv \frac{4}{3}\mathrm{Re}^*$)
H	height of the downstream channel ($\equiv 1.9423$)
r	expansion ratio ($\equiv H/h = 1.9423$)
S	non-dimensional step height ($\equiv r - 1 = 0.9423$)
x_1	length of reattachment for the first floor eddy
x_2	length of separation for the second floor eddy

* Corresponding author. Tel.: +886 2 23625470; fax: +886 2 23929885; e-mail: sheu@indy.na.ntu.edu.tw

0307-904X/99/$ - see front matter
PII: S0307-904X(99)00019-0

x_3 length of reattachment for the second floor eddy
x_4 length of separation for the roof eddy
x_5 length of reattachment for the roof eddy

1. Introduction

As a subject of practical importance in fluid mechanics, flow in channels with reversals has been the focus of intensive study. Examples, among others, are found in heat exchangers, ducts for industrial use, flows around buildings and microelectronic circuit boards. To aid in experimental and computational investigations of this class of flows, the flow past a backward-facing step has been chosen as a representative test bed since it involves a configuration which is regarded as having the simplest geometry. Geometrical simplicity does not imply that the phenomena of the flow are also simple. Among the rich features that attract the interest of researchers are flow separation, reattachment and multiple recirculation regions present in the channel.

For reasons of practical and fundamental importance stated above, numerous numerical results have been published in the literature which are focused on studying the effects of the Reynolds number [1–3] and the expansion ratio [4] on the flow pattern behind the step. Comparatively few studies have been addressed to the upstream and downstream channel lengths which might alter the flow development in the channel [5]. The present transient analysis was undertaken to add to the existing knowledge of backward-facing step flow in the hope of deepening our understanding of expansion flow over a wide range of Reynolds numbers. We restrict ourselves to flows with Reynolds numbers lower than 2500. This avoids the complication of simulating flow turbulence.

Numerical simulation of transport equations in a domain of multiple dimensions also encounters a stability problem, known as oscillatory velocities arising from prevailing flow advection, and an inaccuracy problem, known as the false diffusion error. Our goal is to achieve high-order accuracy without much sacrifice of stability. We apply in this paper a quadratic upwind scheme to approximate the convective flux terms in a domain, which has been non-uniformly discretized. Other spatial derivative terms in the equations are approximated by a centered scheme to obtain second-order accuracy. As to the approximation of time derivative terms, we simply apply the first-order accurate Euler implicit time-stepping scheme. Since discretization errors stemming from the curvilinear coordinate transformation are generally considerable and are hard to resolve for configurations involving complexities or for curvilinear lines having appreciable changes in curvature, we conduct analysis here in a Cartesian coordinate system.

The remaining sections are organized as follows. Working equations which permit specification of closure initial/boundary conditions are given in Section 2, followed by a brief outline of the segregated-type algorithm, and an introduction to the finite volume discretization method employed and the flux discretization scheme adopted. The justification for using this analysis code is presented in Section 3. In Section 4, we describe first the problem under investigation. The Reynolds number used in this study follows the same definition as that given in Armaly et al. [1] to facilitate the direct comparison with the experimental data. Time steps and mesh sizes are also detailed in this section. With the finite volume solutions obtained, we choose the streamline as the target vector field to explore the vortical flow structure by appealing to the theory of topology. A topological study on the computed primitive velocity vectors provides insight into the structure of vortical flows. Finally, we draw conclusions in Section 5.

2. Working equations and numerical method

We consider in this paper Newtonian fluids which are subjected to the incompressibility constraint condition. Together with this divergence-free condition, Navier–Stokes equations representing the equations of motion are cast in the dimensionless form:

$$\frac{\partial u_i}{\partial t} + \frac{\partial}{\partial x_m}(u_m u_i) = -\frac{\partial p}{\partial x_i} + \frac{1}{\mathrm{Re}^*}\frac{\partial^2 u_i}{\partial x_m \partial x_m}, \tag{1}$$

$$\frac{\partial u_i}{\partial x_i} = 0. \tag{2}$$

The idea behind the choice of the above velocity–pressure formulation is that this variable setting accommodates closure conditions [6].

We have transformed the above elliptic–parabolic differential equations into their algebraic counterparts, which are amenable to computer simulation, using the finite volume method. Numerical simulation of incompressible fluid flow, however, encounters spurious pressure modes. This presents a difficulty which can be overcome by adopting the staggered-grid approach [7]. In the staggered-grid approach, grids used offset the velocities by a half mesh width in their respective coordinate direction from the pressure. Such a grid setting facilitates finite volume integration of working equations in their representative volumes where the corresponding primitive variable is stored at the cell center.

The absence of a pressure variable in the constrained working equation (or divergence-free continuity equation) tends to weaken the matrix equations, in the sense that matrix equations become increasingly ill-conditioned. It is this difficulty which motivated us to apply the algorithmic idea of the segregated approach to solve for finite volume discretization equations in an iterative manner. The key to successfully applying the segregated approach is to satisfy the solenoidal kinematic constraint $\nabla \cdot \vec{u} = 0$. In this study, we employ the pressure difference p' as a representative working variable to replace the continuity equation. The resulting Poisson equation for p' is used to compensate the pressure–velocity decoupling. As a direct consequence of this decoupling nature of the working equations, it is appropriate to apply the semi-implicit iterative algorithm, namely SIMPLE-C [8], to solve three momentum equations and one Poisson equation for the pressure difference in a cyclic predict-and-correct process. The solution algorithm is detailed as follows.

In each time step, calculation starts by setting the pressure values to be those just obtained. This is followed by solving three momentum equations to obtain their representative primitive velocities through introduction of under-relaxation E-factors to the discrete equations. We take larger E-factor for the prevailing velocity-component to speed-up the calculation. We also calculate the coefficients shown in the p' equation using the most updated velocities. When solving the Poisson equation for p', we introduce an over-relaxation factor θ, which has a value as high as 1.99. The solution for p' is obtained in an alternating-direction-implicit fashion. As is usual, 4–8 inner iterations are needed. Upon obtaining p', we correct the pressure by adding $\alpha p'$ to the old pressure value. Depending on the E-factors, the free parameter α is not necessarily set to be 1. Having obtained the pressure values, we make a shift of nodal pressures with respect to an arbitrarily referenced nodal pressure. This step is crucial to accelerate convergence of solutions. We then check whether the continuity constraint condition is satisfied. If not, we return to the original outer-iteration step and repeat the calculation. This alternating-direction-implicit calculation terminates until the convergence criterion is reached. In all the cases investigated, the solution was said to have converged when the global pressure and velocity residuals reached a value of 10^{-12}.

A serious problem with flow analyses was the false diffusion error. To remedy this difficulty, a QUICK discretization scheme implemented on non-uniform grid [9] is considered as a refinement to Leonard's original scheme [10] for the spatial discretization. This upwind treatment of advective terms stabilizes the discrete system and provides a numerical scheme that is globally third-order accurate in space. Other spatial derivatives in the equations are approximated using a second-order accurate centered scheme.

3. Verification of analysis code

As a first step toward validation of the use of the computer code developed to simulate the expansion flow in the channel, we conduct here a test problem which is amenable to the analytic solution. The test case is that of the Pearson vortex problem [11]. In a square domain of length 1, we solve for primitive variables, subjected to the boundary values of the velocity and initial condition ($t = 0$) given below:

$$u = -\cos \pi x \, \sin \pi z \, \mathrm{e}^{-2t/\mathrm{Re}}, \tag{3}$$

$$w = \sin \pi x \, \cos \pi z \, \mathrm{e}^{-2t/\mathrm{Re}}. \tag{4}$$

The analytic pressure reads

$$p = -\tfrac{1}{4}(\cos 2\pi x + \cos 2\pi z) \, \mathrm{e}^{-4t/\mathrm{Re}}. \tag{5}$$

We performed calculations under conditions of $\Delta t = 5 \times 10^{-5}$ and $\mathrm{Re} = 10^4$. The uniform mesh sizes we consider in this validation test are with resolutions of 10×10, 20×20, 30×30, and 40×40. After 200 time steps, convergent results obtained at $t = 0.01$ showed increasing agreement with analytical solutions shown in Fig. 1. This validation study provided us with confidence to proceed with the subsequent backward-facing step problem.

4. Computed results

4.1. Problem description and general flow structure

The channel configuration used for this study was that of Armaly et al. [1]. In the channel shown schematically in Fig. 2, there is a built-in backward-facing step with a height of $S = r - 1$. This configuration provides an expansion ratio of $r = H/h = 1.9423$. The larger channel, located just downstream of the step, has a height $H = 1.9423$. In order to make the calculations affordable, the channel is truncated at $x = x_0$, which should be sufficiently distant from the step. According to Armaly et al. [1], the length of x_0 was suggested to be larger than $4x_1$, where x_1 denotes the first floor reattachment length. This chosen length allows the flow to develop into a fully developed profile. We analyzed numerically this problem for a wide range of Reynolds numbers covering simply the laminar flow regime. The definition of the Reynolds number given in (1) is

$$\mathrm{Re}^* = \frac{U_{\max} h}{v}, \tag{6}$$

where the chosen reference velocity $U_{\max}(\equiv 1)$ is the maximum inlet channel velocity (or 1.5 times of the mean inlet velocity), and v is the kinematic viscosity. For this study, $h(\equiv 1)$ is the height of the upstream channel which is chosen as the reference length in the present normalization of working equations. Having chosen the reference velocity, $U_{\max}$, and the reference length, h, we can

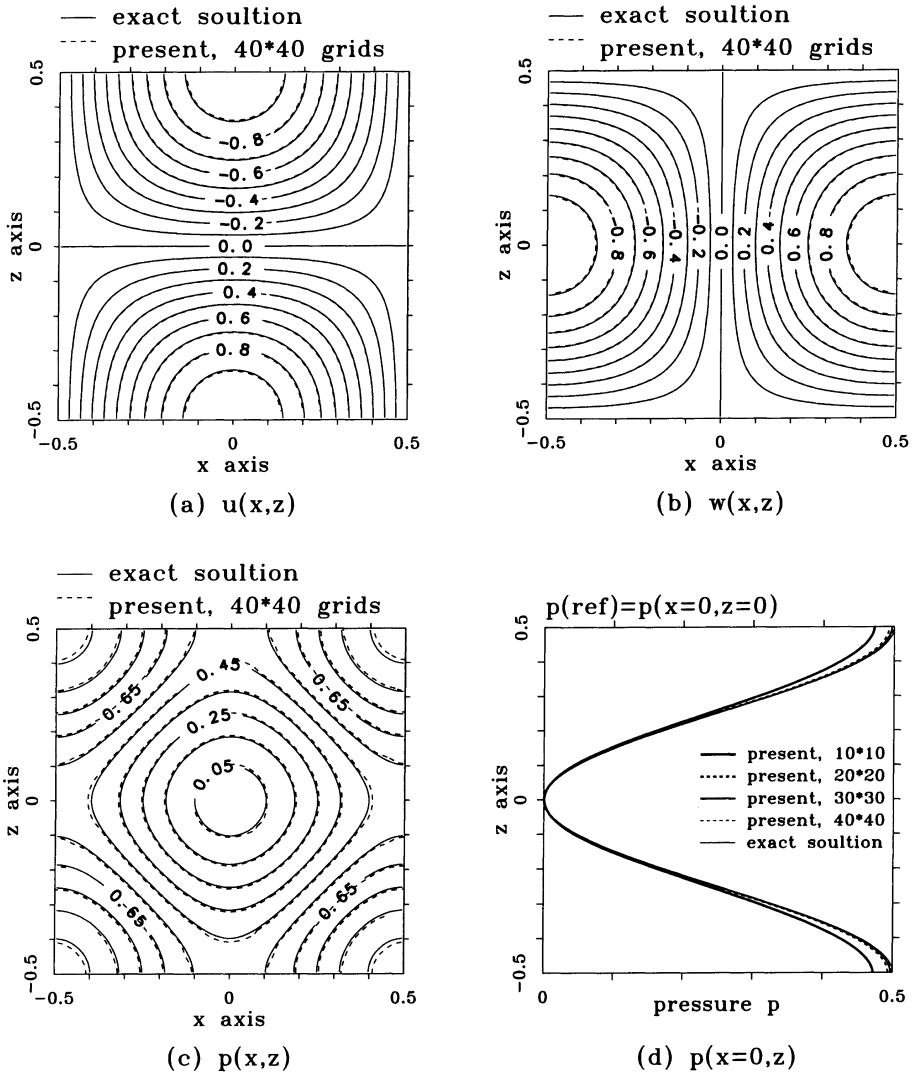

Fig. 1. Code validation for the Pearson vortex problem given in Section 3: (a) $u(x,z)$; (b) $w(x,z)$; (c) $p(x,z)$; (d) grid convergent test on $p(x=0,z)$.

normalize the pressure by $\rho U_{\max}^2$ and the time by $h/U_{\max}$. The density of the fluid, ρ, remains unchanged with time and space in the present incompressible flow simulation. In what follows, the discussion of results is based on the Reynolds number Re, given by Armaly et al. [1], which is, by definition, equal to $\frac{4}{3}\mathrm{Re}^*$.

To close the mixed set of partial differential equations (1) and (2), we prescribe a fully developed velocity profile at the channel inlet but a Neumann type boundary condition at the truncated outlet plane. The chosen outflow velocity boundary condition is of the zero-gradient type. Along the solid boundaries, the usual no-slip boundary conditions apply. For physical reasons, grids, as shown in Fig. 2, are refined near the step plane, roof, and floor of the channel to resolve the high-gradient boundary layer profile. Along the primary flow direction, x, and the transverse direction, z, the extreme grid sizes are with the values of $\Delta x(\min,\max) = (0.03, 1.0)$ and $\Delta z(\min,\max) = (0.03, 0.06)$, respectively.

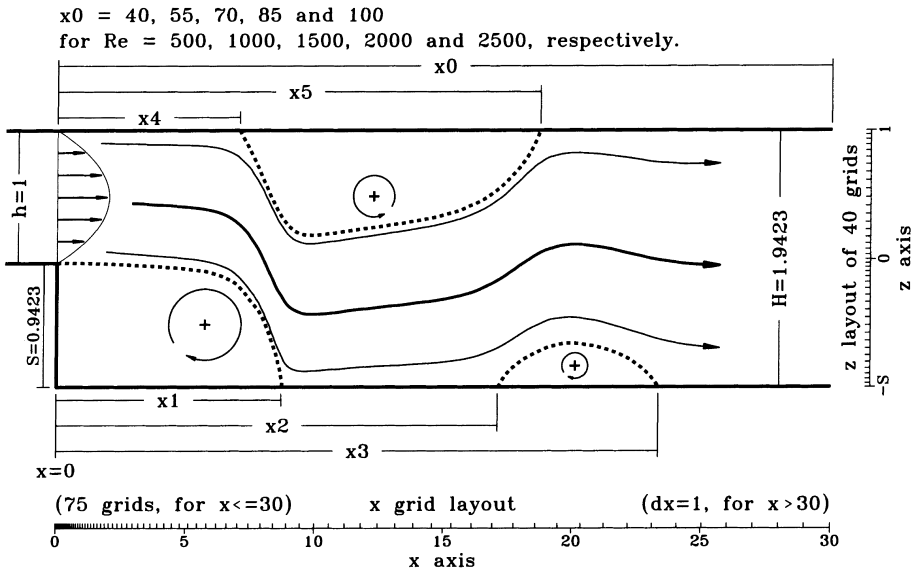

Fig. 2. Illustration of the geometry of the two-dimensional channel with a backward-facing step. The physical domain has been non-uniformly discretized with a mesh of 145×40 for the Reynolds number Re at 2500.

The aim of this study was to provide insight into the time evolution of the developed vortical flow as there is still much to be learnt from the computed time-accurate solutions. We start the calculation at $u = v = 0$. The time increment used in the Euler implicit time-stepping scheme varies with the time. The detailed time intervals are tabulated in Table 1. In our study, time-accurate solutions obtained within each time step are that the mass flow rate at every cross-section, Q, must reach $|Q - Q_0|/Q_0 < 10^{-6}$ where Q_0 is the inlet mass flow rate. The iteration numbers needed to achieve the convergent solutions within a typical time step are tabulated in Table 1 for the reader's reference. We have justified the use of time steps tabulated in Table 1 for the present study through the time-step refinement test. By cutting the time step by half, the maximum difference between the solutions computed under finer time-step conditions and those presented in this paper is less than 4% in the time interval of $0 \leqslant t \leqslant 40$. As $t > 60$, two computed solutions are essentially the same. This time-step refinement study shows the appropriate choice of the time steps tabulated in Table 1 for Reynolds numbers in the range of $50 \leqslant \mathrm{Re} \leqslant 2500$. We now provide evidence that within each time step

Table 1
Time increments chosen in the transient analysis

t	Δt	Iteration number needed
0–0.2	0.005	~1500
0.2–1	0.025	~1000
1–5	0.05	~500
5–20	0.1	~250
20–50	0.25	~200
50–500	0.5	~150
500–1000	1	~100
1000–5000	2.5	~50
5000–10000	2.5	~20

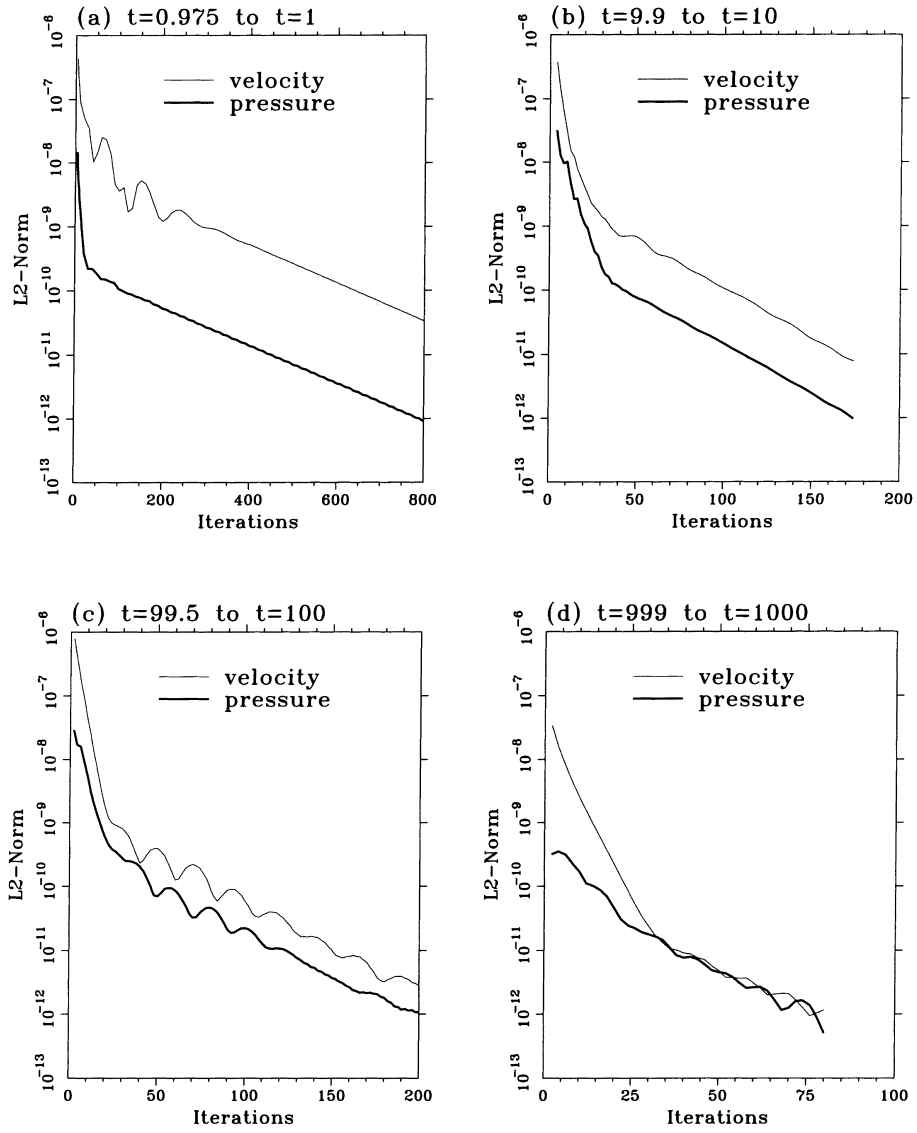

Fig. 3. Error reduction plots for showing convergent solutions are indeed obtained for the case of Re = 2500: (a) from $t = 0.975$ to $t = 1$; (b) from $t = 9.9$ to $t = 10$; (c) from $t = 99.5$ to $t = 100$; (d) from $t = 999$ to $t = 1000$.

working variables converge to their time-accurate solutions. Due to space consideration, we only show in Fig. 3 that solutions are indeed convergent at $t = 1$, 10, 100 and 1000 for the case of Re = 2500.

As is usual, we compared the present solutions with experimental solutions that are available in the published literature. A comparison was made by plotting the streamwise velocity profiles in Fig. 4 for different Reynolds numbers, namely Re = 100, 389 and 1000. This comparison shows a good agreement with the data of Guerrero and Cotta [12]. As to the comparison with the experimental data, it is found a good agreement with reliable data [1] at least for Reynolds numbers lower than 450, further confirming the validity of the finite volume code presented in the previous section. The difference between two sets of data computed for the case of is mainly attributed to the omission of y-coordinate in the analysis.

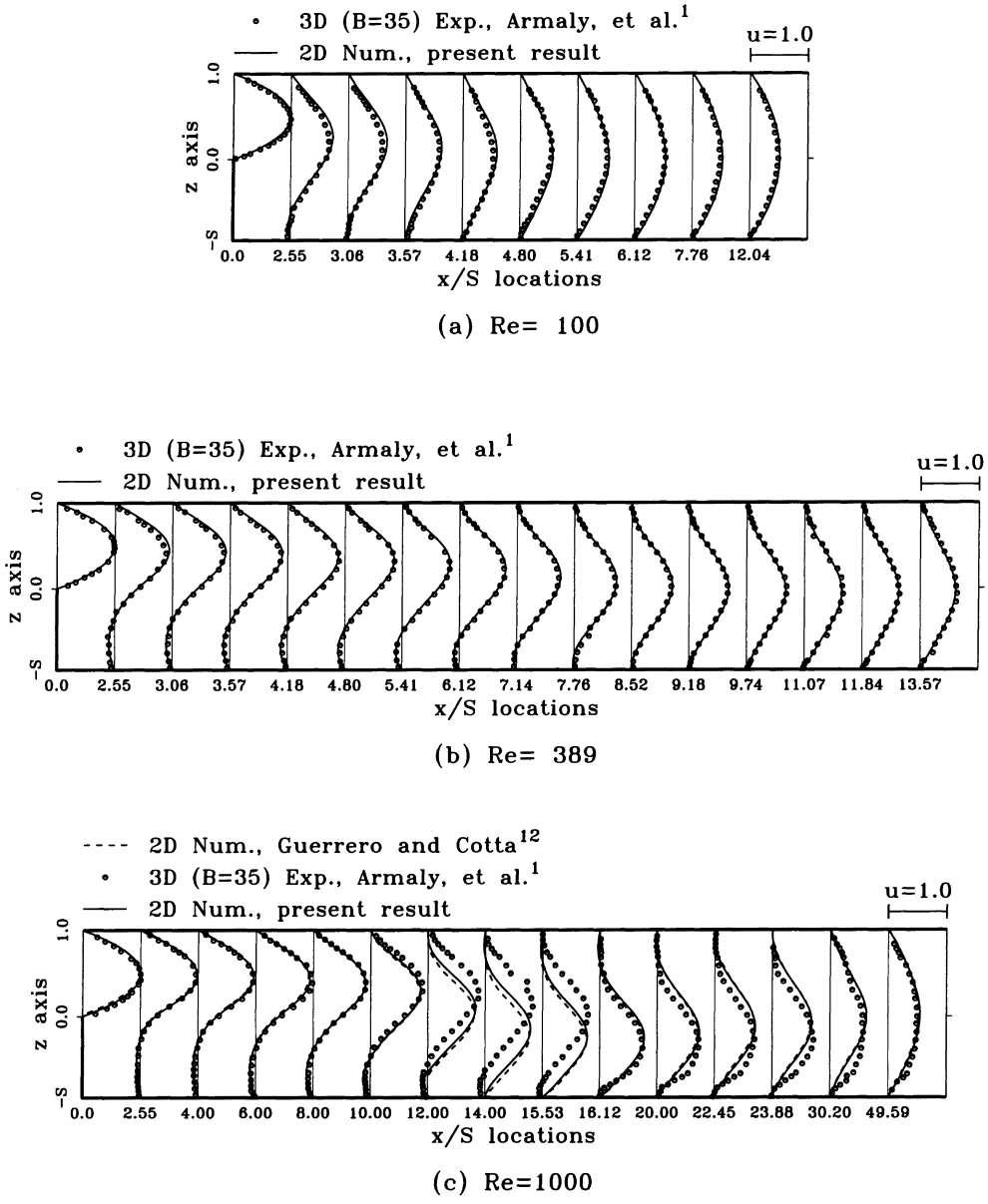

Fig. 4. Comparison of the computed streamwise velocity profiles with the experimental results of Armaly et al. [1] and the numerical results of Guerrero and Cotta [12]: (a) Re = 100; (b) Re = 389; (c) Re = 10000.

Among the basic flow features pertinent to the investigated channel is the flow separation from the step corner. As can be seen in Fig. 5, the flow is essentially a potential flow in the startup stage, at which a no-slip condition is impulsively imposed on the step plane. A sudden change in the streamwise velocity at the upper corner of the step plane causes a vortex to form, as seen in Fig. 5 at $t = 1$. This local shear-induced vortex, affected by the dissipative nature of the fluid viscosity, convects downstream. As bounded by the step plane, the channel floor and the inlet high-momentum flux, the vortex is forced to move downward in its subsequent evolution.

The points at which the flow reattaches and separates are crucial to determine the recirculating zone. We determine these points using the theory of topology [13], which will be discussed

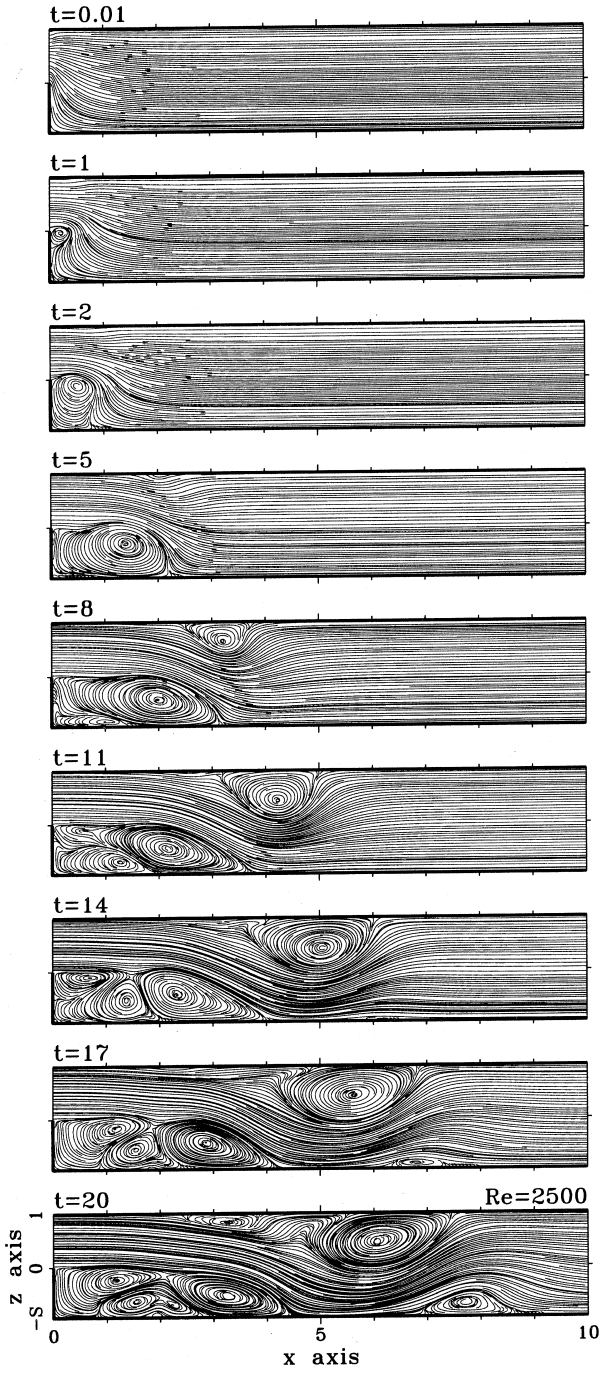

Fig. 5. Computed streamlines during the transient development phase, between $t = 0.01 \sim 20$ for the case of $\mathrm{Re} = 2500$.

later. With the point of separation in the step corner and the point of reattachment on the floor, a zone of flow reversal is formed immediately behind the step. Since flow reversals in the primary eddy have significant impact on the hydrodynamics and heat transfer rates, it is worthwhile to clarify the extent of these flow reversals. We thus plot reattachment lengths x_1, as scaled with the step height S, against Reynolds numbers in Fig. 6. Clearly seen from this figure is that

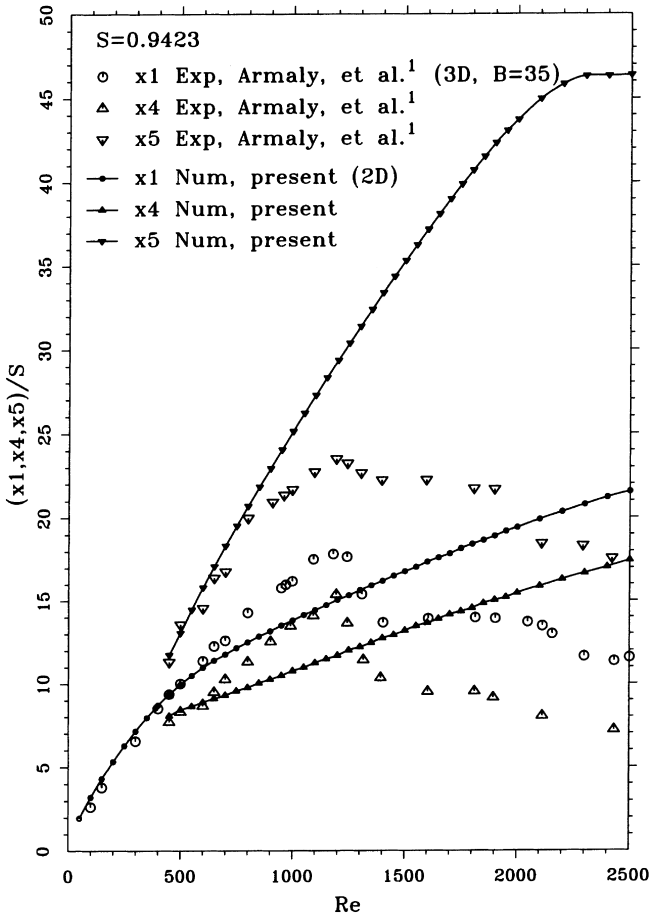

Fig. 6. Comparison of experimental (Armaly et al. [1], with the channel width of $B = 35$) and numerical (present, 2D) results for the reattachment lengths x_1 and x_5 and separation length x_4 for Reynolds numbers no larger than $\mathrm{Re} = 2500$.

the normalized reattachment length increases linearly with the Reynolds number. For Reynolds numbers less than 600, these normalized reattachment lengths compare favorably with experimental data [1]. While discretization errors due to false diffusion are unavoidable, the difference in x_1 between the present numerical calculation in finer grids and the experimental measurement can be explained as being caused by the three dimensionality of the flow where the vortex stretching term is significant [14]. For laminar flows in the range of $0 \leqslant \mathrm{Re} \leqslant 450$, we referred to them as being essentially self-similar in the sense that the computed normalized reattachment lengths lie on a single curve.

With the primary eddy being stably formed behind the step, the expansion flow has a tendency to curve toward the channel roof, thus forming a family of convex streamlines. Along the channel roof, the bending streamlines have a tendency to form a new separation zone containing flow reversals. The rotation direction is, however, opposite to that found in the main bubble behind the step plane. Unlike the primary eddy, this secondary separation eddy is formed due to the adverse pressure gradient in association with the expansion flow created by a sharp change in the channel sectional area. This eddy was observed experimentally first by Armaly et al. [1] and was later confirmed numerically by Kim and Moin [15]. According to our computation, the secondary eddy is not steadily attached to the channel roof until the Reynolds number increases to 450. It is, however, important to note that in the course of flow development the secondary eddy does

appear at a Reynolds number with a value much small than 450. In the early transient period, the presence of such eddy is gradually dissipated by the fluid viscosity. The curved streamlines formed over the channel roof provide a mechanism opposing flow reattachment to the channel floor and, thus, preventing the continuous increase of the length of x_1.

Before closing this section, we present a parametric study by varying the Reynolds number, with an aim to know at what Reynolds number the new recirculating bubbles burst. Numerical exercises reveal that at Reynolds number 400, the separation-reattachment flow pattern is not observed near the channel roof. With an increase of Reynolds number up to $\mathrm{Re} = 450$, the recirculating region attached to the channel roof becomes visible. At the Reynolds number $\mathrm{Re} = 500$, this eddy, as shown in Fig. 7, is clearly revealed. When the Reynolds number increases continuously to 2100, the second separation-reattachment phenomenon at the channel floor is found. For a clear representation of eddy formation, we present computed flowlines for $\mathrm{Re} = 500$, 1000, 1500, 2000 and 2500 in Fig. 7.

While the steady-state eddies, as shown in Fig. 7, are quite simple in their structure, the flow physics is rather complex. Physical complexities are attributable to the eddy formation and mergence. In support of what we claimed, we adopted the theory of topology [13] to find critical points from the computed velocity field. Due to space consideration, we only plot in Fig. 8 critical points for the case of $\mathrm{Re} = 2500$ at $t = 80$. There exist 44 critical points which fall into topological types shown in this figure.

4.2. A detailed description of flow evolution

The geometry of the channel that is used for this study is simple. Nevertheless, the flow structure which evolves in the wall-bounded channel is fairly complex. Our interest in this section

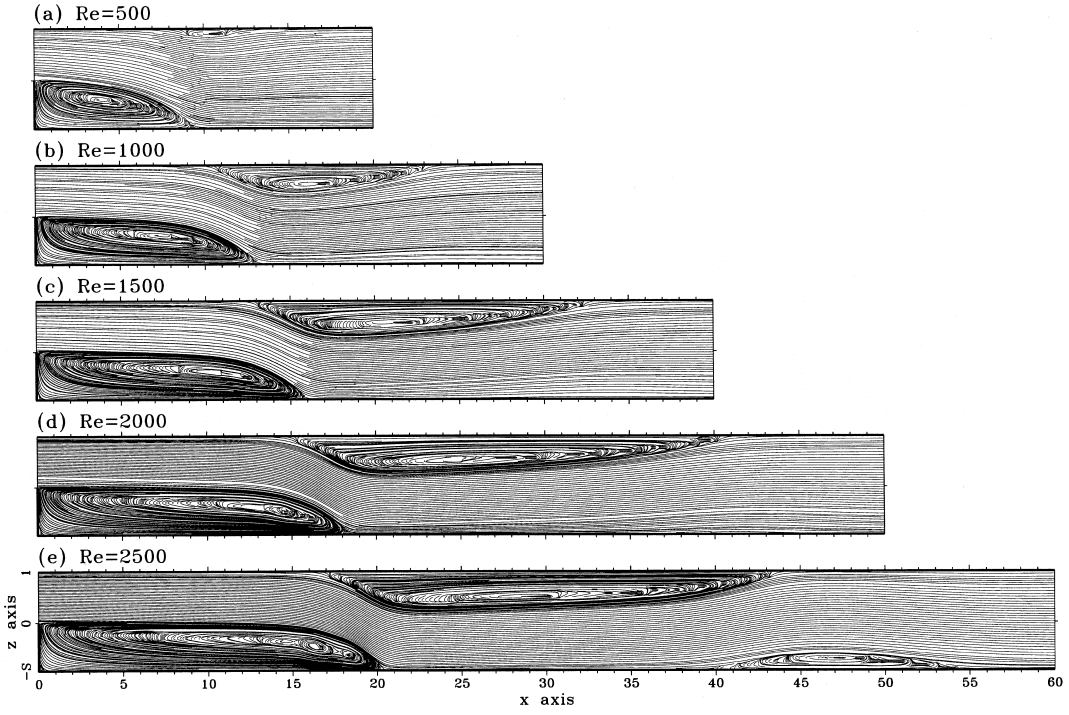

Fig. 7. Computed streamlines at different Reynolds numbers: (a) $\mathrm{Re} = 500$; (b) $\mathrm{Re} = 1000$; (c) $\mathrm{Re} = 1500$; (d) $\mathrm{Re} = 2000$; (e) $\mathrm{Re} = 2500$.

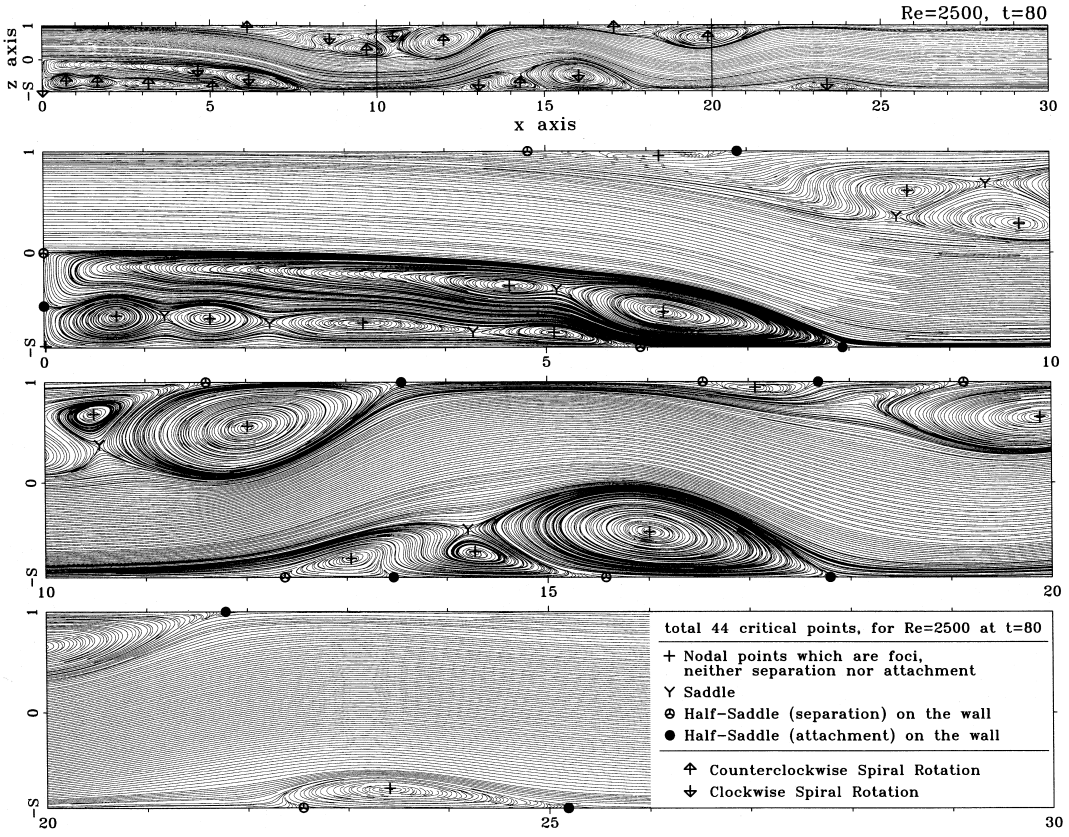

Fig. 8. Topological flow structure at $t = 80$ for the case of $\mathrm{Re} = 2500$.

is to provide a complete picture of the startup flow structure downstream of the step. Due to space considerations, flow complexities were shown only for the Reynolds number $\mathrm{Re} = 2500$ to deepen our insight into the expansion flow structure in the channel.

For illustration purposes, we plot flow lines (or instantaneous streamlines) in Figs. 5 and 9. By definition, flow lines are locally tangent to the computed vector field. These lines, thus, help to reveal the inherent vortical flow structure. As can be seen in Fig. 5, the impulsively started flow over a step has a nominally potential flow character which was experimentally confirmed [16]. Also, this essentially elliptical flow pattern can be theoretically supported by adopting the Batheman principle [17] and its extension to viscous flow [18]. According to Ecer et al. [19], velocity vectors in the Navier–Stokes equations can be decomposed into a potential part, $\nabla\phi$, irrotational part, $s\nabla\eta$, and, lastly, second-order tensor dissipative attributions. Here, ϕ, s, η are the velocity potential, entropy and Lagrangian multiplier, respectively. In the startup stage, the flow becomes rotational in regions immediately adjacent to the step corner. The flow is regarded as being nominally irrotational under these circumstances. Even subject to sudden imposition of a no-slip condition on the channel wall, the flow is essentially not affected by the fluid viscosity in the impulsively starting stage. These theoretically plausible reasons explain why the startup flow is characterized as having a potential nature.

To study the time-varying flow physics, we plot a sequence of frames of streamlines, starting from $t = 0$ and terminating at the dimensionless time $t = 10^4$, for the case with $\mathrm{Re} = 2500$. A concentrated single vortex around the step corner is found from these figures. The shed vortex is convected with the expansion flow and moves toward the downstream channel floor. While this

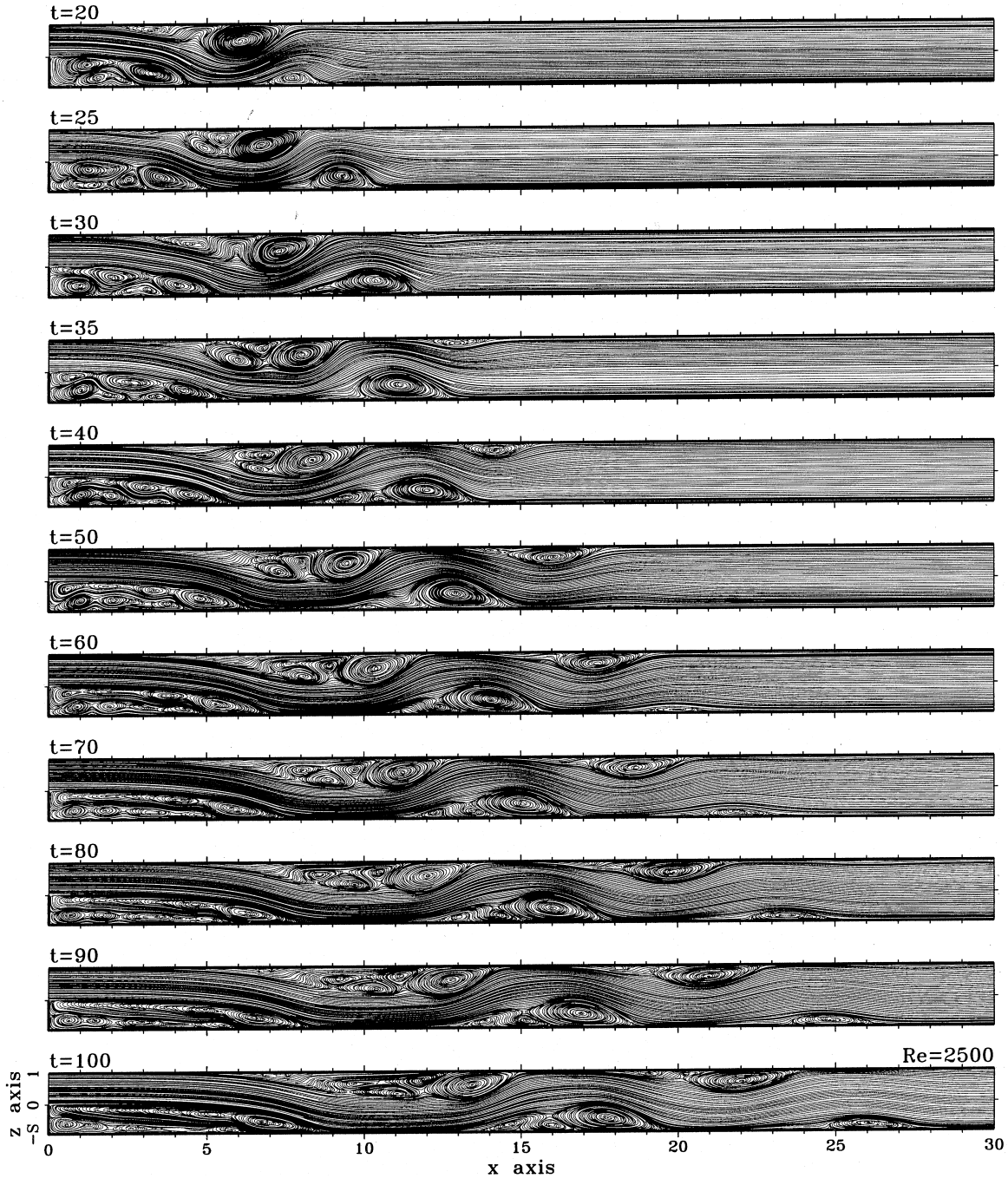

Fig. 9. Computed streamlines in the time range of $t = 20 \sim 10000$ for the case of $\mathrm{Re} = 2500$.

shed vortex is subjected to fluid viscosity and is, thus, dissipated, the vortical flow is strengthened by the flow entrainment from the inlet flow which undergoes an expansion process. Part of the fluid moves upstream and enters into the recirculation zone, and this increases the extent of the primary flow regime. As seen in Fig. 10, the reattachment length x_1 increases monotonically with time for the case of $\mathrm{Re} = 2500$ and gradually approaches its asymptotic value at a time near $t = 2000$. Here, the reattachment point is defined as the point which is determined from two most

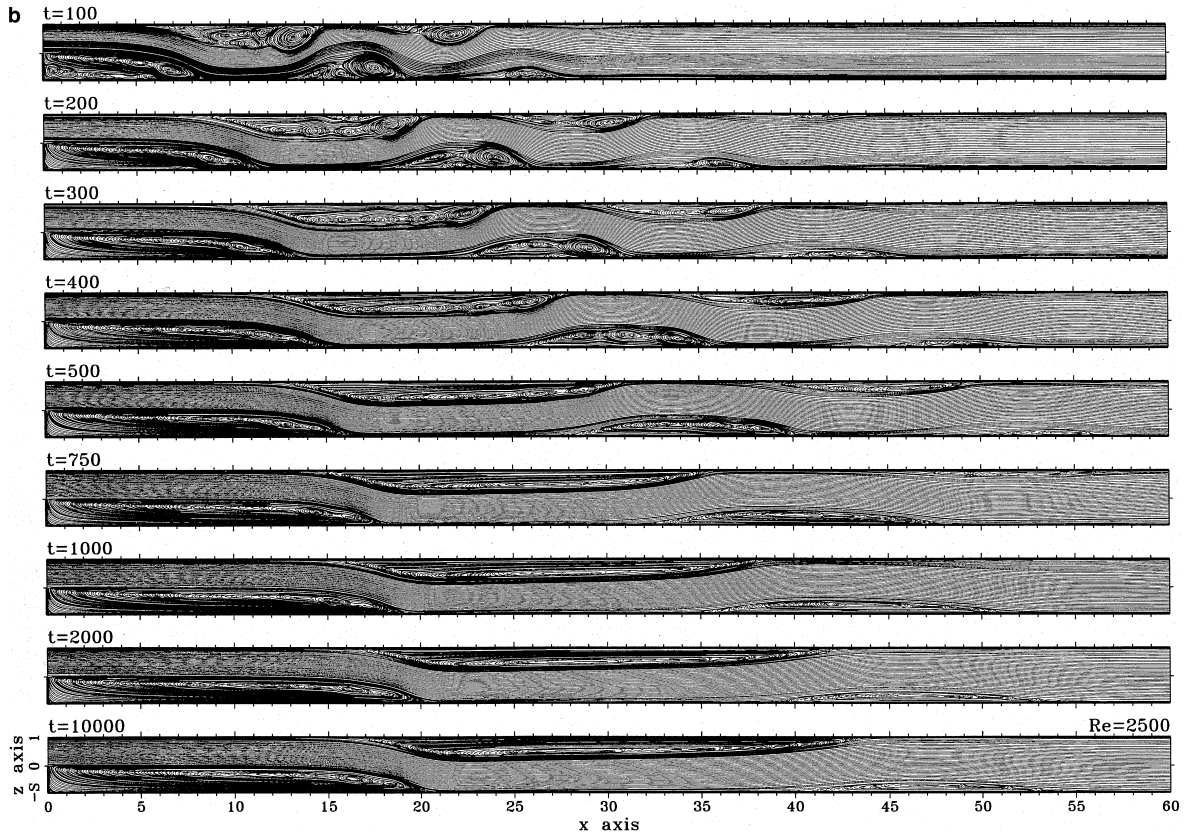

Fig. 9. Continued.

adjacent solution points, at which the velocity component u changes sign, and is extrapolated to the location at the channel floor.

Flow entrainment gradually intensifies the vortex and extends its vortical regime toward the channel floor, thus forming a single, elliptical recirculation eddy behind the step. According to Fig. 9, this primary recirculating bubble is essentially stationary. The primary eddy behind the step develops progressively, leading to convex streamlines which gradually generate an adverse pressure gradient along the channel roof. As time advances to $t > 5$, the secondary eddy becomes clearly visible in Fig. 5. Unlike the mechanism leading to the primary eddy formation behind the step, the secondary eddy forms due to adverse pressure created by the sudden step expansion. For Reynolds numbers higher than 450, once the secondary eddy forms at the channel roof, it will persist in its subsequent flow evolution. The length of x_5, as seen in Fig. 10, also increases smoothly with an increase of time up to $t = 4000$, at which point an asymptotic value of 46.4 is reached. It is worth noting that the time needed for x_1, x_3 and x_4 to reach their asymptotic values is approximately the same. As to values of x_2 and x_5, they slowly evolve to their asymptotic values at a time around $t = 4000$. As $t > 5000$, the flow is essentially at the steady state.

As time advances to $t = 8$, as shown in Fig. 5, a new vortex with its rotating direction opposite to that of the primary vortex forms in the region bounded by the primary eddy and the solid walls, comprising the step plane and the channel floor. As $t > 11$, another eddy which splits from the primary eddy forms in the region above the corner eddy. For three eddies configured in this manner, a saddle point emerges in the primary recirculating bubble. The eddy in the vicinity of the

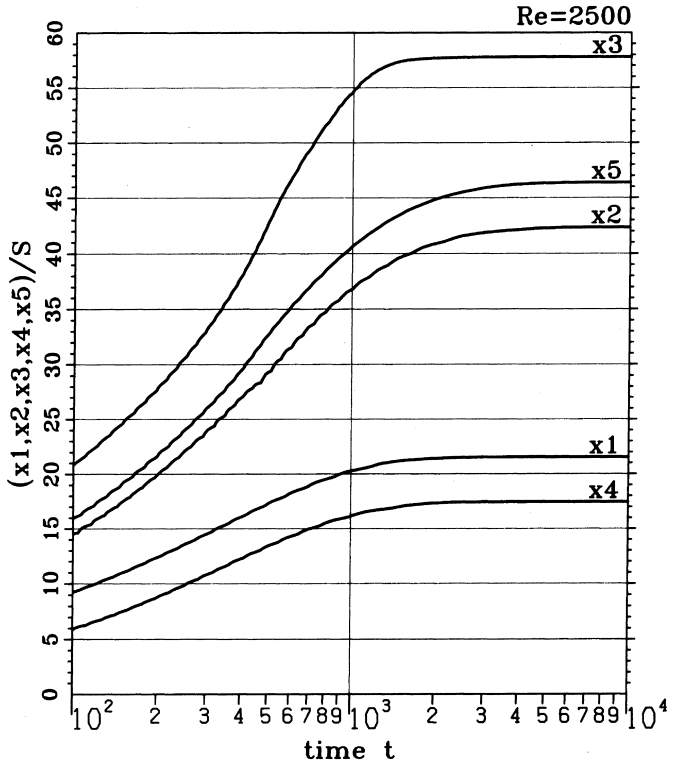

Fig. 10. Time history of the reattachment lengths x_1, x_3, x_5 and the separation lengths x_2, x_4 for the case of Re = 2500.

step corner enlarges with time and compresses the eddy at the intersection of two walls which are perpendicular to each other. According to the solutions computed at Re = 2500, a third recirculating bubble forms at the bottom plane and becomes clearly visible at $t = 17$. This eddy has been experimentally confirmed and is known to cause streamwise adverse pressure gradients to form on the channel floor.

As time goes by, the roof eddy persists in the subsequent evolution and changes its pattern by showing a new counter-rotating pair of vortices which trail behind the original secondary eddy. Three eddies arranged in this form, as shown in Fig. 9 at $t = 25$, pave the way for the second saddle formation in the channel. The middle eddy in the primary circulation bubble splits into two eddies with rotation directions opposite to each other. Like the two other recirculating bubbles, the third bubble formed at the channel floor sheds two smaller trailing eddies at $t = 30$. After another $\Delta t = 5$, the flow has a tendency to detach from the upper wall due to the concave curved flowlines and the established adverse pressure gradient. According to the rotation direction of five small eddies in the primary bubble, three saddles are visible at $t = 40$. Within the primary recirculation zone, eddies increase in number of pairs but are more stretched. For example, there exist seven smaller eddies in the primary bubble at $t = 50$. Later on, the third floor recirculating bubble can be clearly visible at $t = 80$. Multiple small eddies merged. Owing to the fluid viscosity, such an eddy mergence regularizes the flow pattern in the eddy formed immediately behind the step shown in Fig. 8, which plots the solution at $t = 80$.

As Fig. 9 shows, the flow for Re = 2500 gradually approaches its steady-state. Compared with these impulsively started flow patterns, the eddy structure within each recirculating bubble becomes increasingly simple, and the flow gradually becomes steady. We selected points (x, z), as marked by + in Fig. 11(a), and ploted the velocity as a function of time shown in Fig. 11(b). This

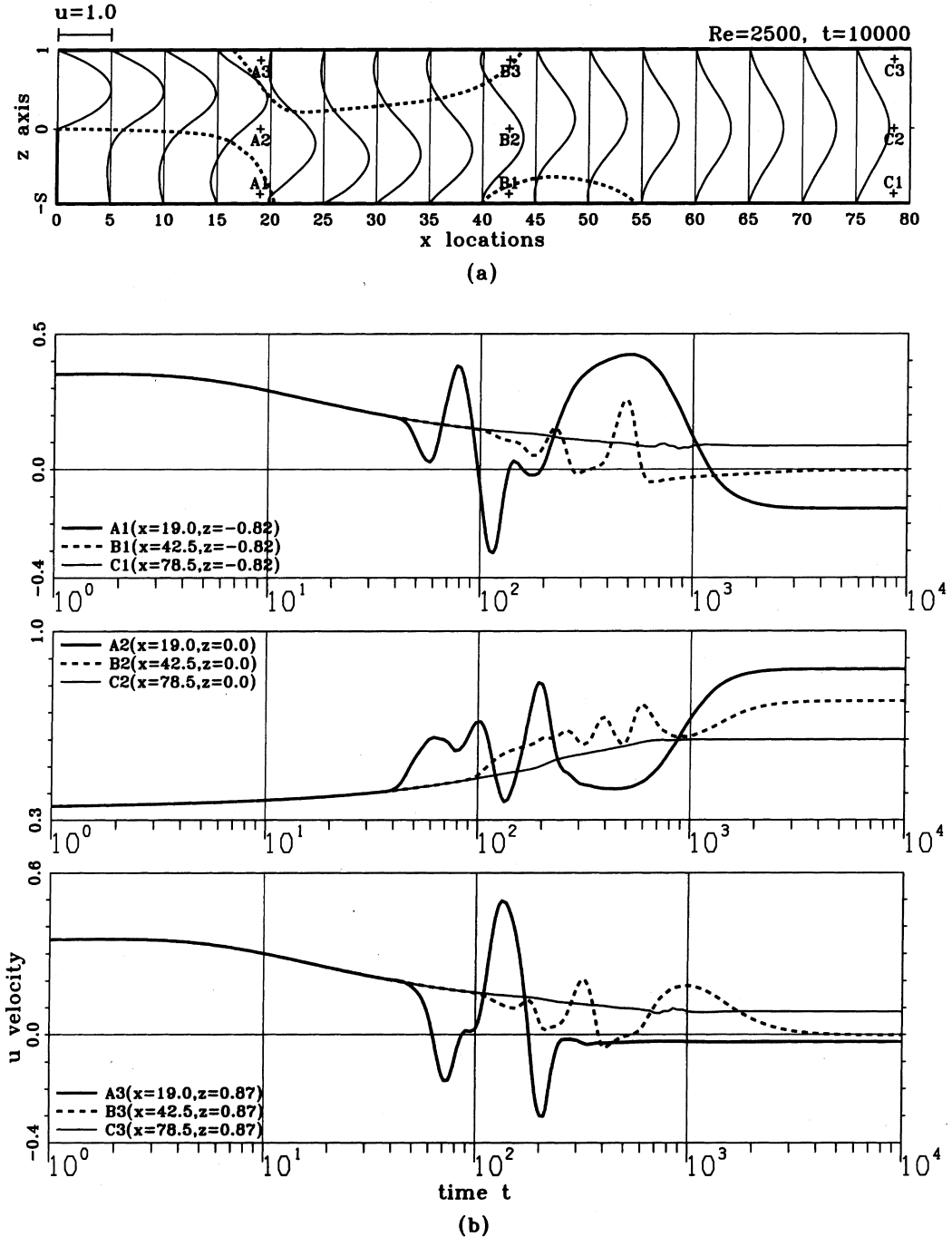

Fig. 11. Computed streamwise velocities at Re = 2500: (a) At different x locations for the $u(x, y, 10000)$; (b) Time history for points marked in Fig. 11(a).

helps us to show the existence of flow steadiness at a time $t > 2000$. To give readers a complete picture of the eddy shedding, it is instructive to plot in Fig. 12 the pressure distribution along the floor, roof and the step of the channel, respectively. Plots shown in Fig. 12 help to confirm the formation of time-varying secondary eddies and their progression in the channel.

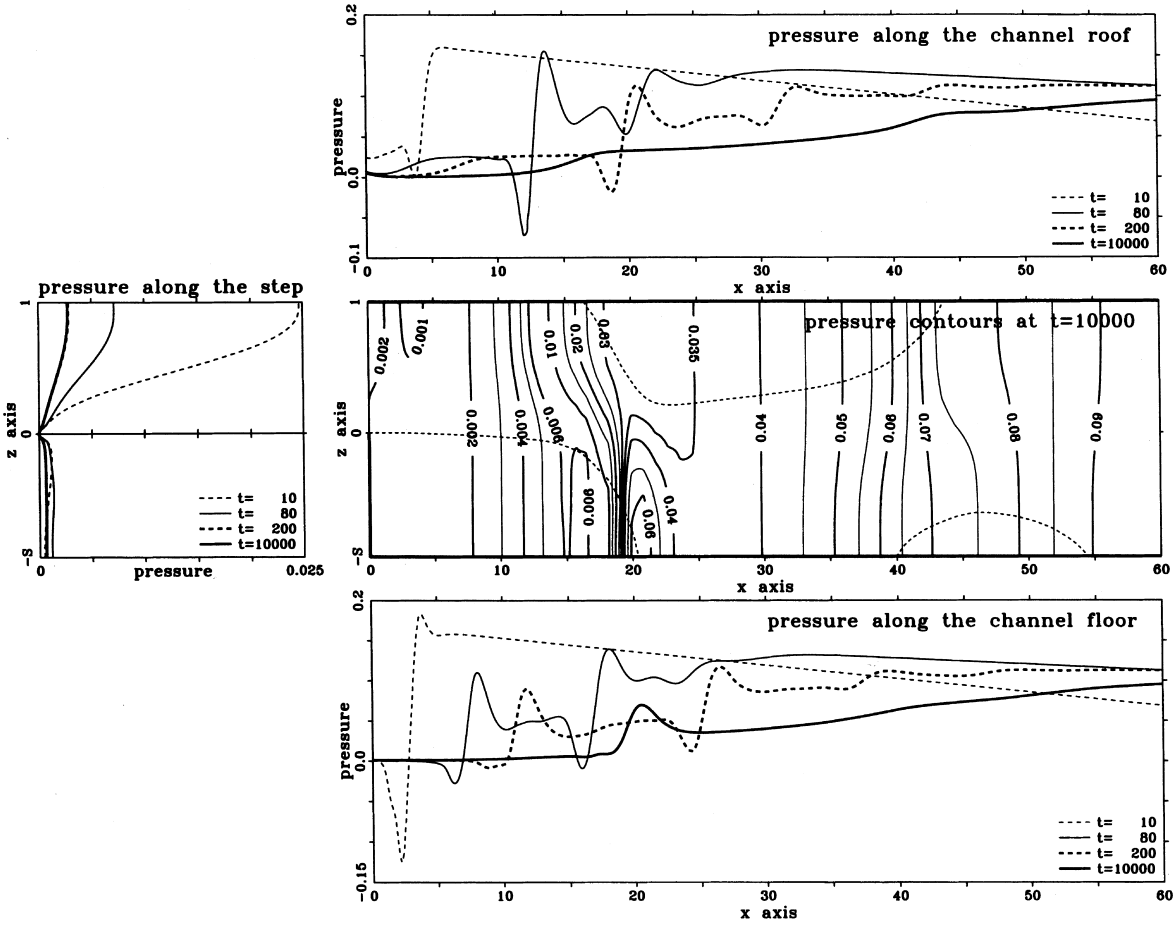

Fig. 12. Computed pressure distribution along the channel floor, roof and the step.

5. Concluding remarks

It is the objective of the current study to add to the existing knowledge about expansion flow structure in the channel with a backward-facing step. The computed results lead to the conclusion that the laminar flow shows an elliptically potential nature in the very beginning of flow expansion. This is followed by increasingly important flow vorticity. Laminar flow with a concentrated vorticity near the step corner separates from the step and convects with the instantaneous streamlines and reattaches to the channel floor. The accompanying curved streamlines form a new separation zone containing recirculation fluids along the channel roof. The adverse pressure gradient causes this roof eddy to form and will persist throughout the entire evolution since $t = 5$. Afterwards, flowlines differ in their opposite curvatures. An environment leading to downstream vortex sheddings, with increasing intensity, is thus established. Within the primary eddy as well as in each adverse pressure gradient induced recirculating bubble, smaller eddies emerge among themselves in a way that saddle points are seen. Using the theory of topology, the flow can be sketched, providing detailed information on the flow structure by virtue of computable topologically critical points. Close examination of the computed solutions reveals that the flow will evolve to its steady state for all the investigated Reynolds numbers.

Acknowledgements

This work was supported by the National Center for High-performance Computing under Grant NCHC 85-04-004. The authors would like to acknowledge one of the reviewers who pointed out mistakes and provided useful comments in his review of the paper.

References

[1] B.F. Armaly, F. Durst, J.C.F. Pereira, B. Schonung, Experimental and theoretical investigation of backward-facing step, J. Fluid Mech. 127 (1983) 473–496.
[2] K. Morgan, J. Periaux, F. Thomasset (Eds.), Analysis of Laminar Flow Over a Backward Facing Step, in: Proc. GAMM wkshp, Bievres, France, 1983.
[3] A.F. Ghoniem, Y. Cagnon, Vortex simulation of laminar recirculating flow, J. Comput. Phys. 68 (1987) 346–377.
[4] T. Thangam, D.D. Knight, Effect of stepheight on the separated flow past a backward facing step, Phys. Fluids A1 (3) (1989) 604–606.
[5] L. Kaiktsis, G.EM Karniadakis, S.A. Orszag, Onset of three-dimensionality, equilibria, and early transition in flow over a backward-facing step, J. Fluid Mech. 231 (1991) 501–528.
[6] O.A. Ladyzhenskaya, Mathematical problems in the dynamics of viscous incompressible flow, Gordon and Breach, New York, 1963.
[7] F.H. Harlow, J.E. Welch, Numerical calculation of time-dependent viscous incompressible flow of fluid with free surface, Phys. Fluids 8 (1965) 2182–2189.
[8] J.P. Van Doormall, G.D. Raithby, Enhancements of the SIMPLE method for predicting incompressible fluid flows, Numer. Heat Transfer 7 (1984) 147–163.
[9] T.P. Chiang, R.R. Hwang, W.H. Sheu, Finite volume analysis of spiral motion in a rectangular lid-driven cavity, Int. J. Numer. Meth. in Fluids 23 (1996) 325–346.
[10] B.P. Leonard, A stable and accurate convective modeling procedure based on quadratic upstream interpolation, Comput. Meth. Appl. Mech. Engrg. 19 (1979) 59–98.
[11] A.J. Chorin, Numerical solution of the Navier–Stokes equations, Mathematics of Comput. 22 (1968) 745–762.
[12] J.S. Perez Guerrero, R.M. Cotta, Benchmark integral transformation results for flow over a backward-facing step, Comput. Fluids 25 (5) (1996) 527–540.
[13] J.C.R. Hunt, C.J. Abell, J.A. Peterka, H. Woo, Kinematical studies of the flows around free and surface-mounted obstacles; applying topology to flow visualization, J. Fluid Mech. 88 (1) (1978) 179–200.
[14] J.A. Sethian, A.F. Ghoniem, Validation study of vortex methods, J. Comput. Phys. 74 (1988) 283–317.
[15] J. Kim, P. Moin, Applications of a fractional-step method to incompressible Navier–Stokes equations, J. Comput. Phys. 59 (1985) 308–323.
[16] H. Honji, The starting flow down a step, J. Fluid Mech. 69 (1975) 229.
[17] H. Bateman, Notes on a differential equation which occurs in the two-dimensional motion of a compressible fluid and the associated variational problem, Prof. Roy. Soc., London, Sec. A., 125 (1929) 799.
[18] W.H. Sheu, A variational finite element method for three-dimensional, steady, compressible, viscous flows, PhD dissertation, Department of Mechanical Engineering, Purdue University, 1987.
[19] A. Ecer, H.U. Akay, W.H. Sheu, A variational finite element formulation for viscous compressible flows, Numerical methods for compressible flows-finite difference, element and volume techniques, ASME AMD 78 (1986) 5–17.